



ACADÉMIE
DES SCIENCES
INSTITUT DE FRANCE

Comptes Rendus

Chimie

Ephraim Akuaden Audu, Adebola Femi Ade-Ajayi, Aisha Ayoola Osigbesan,
Zaharaddeen Sani Gano and Jeffrey Tsware Barminas


**FeO–alumina catalyst for reforming waste polyethylene terephthalate (PET)
pyrolyzed products: synthesis, characterization, and performance evaluation**

Published online: 7 November 2024

Part of Special Issue: Materials and Energy Valorization of Biomass and Waste: The
Path for Sustainability and Circular Economy Promotion

Guest editors: Mejdí Jeguirim (Université de Haute-Alsace, Institut de Sciences des
Matériaux de Mulhouse, France) and Salah Jellali (Sultan Qaboos University, Oman)

<https://doi.org/10.5802/crchim.343>

 This article is licensed under the
CREATIVE COMMONS ATTRIBUTION 4.0 INTERNATIONAL LICENSE.
<http://creativecommons.org/licenses/by/4.0/>



*The Comptes Rendus. Chimie are a member of the
Mersenne Center for open scientific publishing*
www.centre-mersenne.org — e-ISSN : 1878-1543



Research article

Materials and Energy Valorization of Biomass and Waste: The Path for Sustainability and Circular Economy Promotion

FeO–alumina catalyst for reforming waste polyethylene terephthalate (PET) pyrolyzed products: synthesis, characterization, and performance evaluation

Ephraim Akuaden Audu^{®,*}, Adebola Femi Ade-Ajayi[®], Aisha Ayoola Osigbesan[®], Zaharaddeen Sani Gano[®] and Jeffrey Tsware Barminas[®]

^a National Research Institute for Chemical Technology, Basawa, Zaria, Kaduna State, Nigeria

E-mails: akuadenu@gmail.com, ephraim.audu@narict.gov.ng (E. A. Audu)

Abstract. The growing rate of plastic pollution in Nigeria and across the globe, coupled with the need to harness such waste for useful purposes, is a pressing global concern. In this study, a new type of catalyst was synthesized by incorporating mesoporous FeO onto aluminium oxide trihydrate (alumina) and applied in reforming polyethylene terephthalate (PET) pyrolyzed gas into valuable fuels. The pyrolysis process was carried out at 500 °C while vapor reforming was carried out using 0.5 g of catalyst loading in a fixed bed reactor at 450 °C for 90 min. Scanning electron microscopy analysis of catalysts revealed particle sizes of 1.42–7.63, 1.37–10.75, and 2.66–6.34 μm for alumina, 3% FeO/Al, and 5% FeO/Al, respectively. The percentage compositions of Fe in the synthesized catalyst from the X-ray fluorescence results were found to be 4.7% and 3.62% for 5% FeO/Al and 3% FeO/Al, respectively. XRD analysis revealed that the synthesized catalysts were non-crystalline. Catalyst performance evaluation from the gaseous product revealed a decrease in oxygen from 23.3% in the blank run to 5.33% in 5% FeO/Al. The H₂ content was found to be highest in 5% FeO/Al with a value of 17.14% while the CH₄ content was found highest in 3% FeO/Al (16.22%). Fourier transform infrared analysis of the liquid products inferred peaks corresponding to aromatic and saturated hydrocarbons, which was confirmed by gas chromatography mass spectrometry analysis. Findings from this research demonstrated that the synthesized catalyst was able to reform waste PET pyrolyzed gas into valuable products, addressing environmental challenges and providing alternative energy sources.

Keywords. Catalyst, FeO, Polyethylene terephthalate, Pyrolysis, Reforming, Plastic waste.

Funding. National Research Institute for Chemical Technology (NARICT) under project number FGN/AB2021/ERGP30122610.

Manuscript received 4 March 2024, revised 6 June 2024 and 17 July 2024, accepted 17 September 2024.

1. Introduction

The increasing global production and use of plastics, such as polyethylene terephthalate (PET),

polyethylene (PE), polystyrene (PS), and others, have led to growing concern about environmental pollution and waste management. Nigeria is the most populous country in Africa, located at the west African subregion. It holds a land area of 932,768 km²

*Corresponding author

with an estimated population of 211.4 million [1]. According to Sogbanmu [2], Nigeria ranks ninth globally among countries with the highest contributions to plastic pollution, producing 2.5 million tons of plastic waste annually [3]. Furthermore, over 88% of the plastic waste generated is not recycled, suggesting that such waste is not properly managed. Currently, most plastic waste in the country is dumped at sites and landfills or incinerated. Improper disposal of plastic waste can lead to the leaching of toxic additives into water bodies, blocking of drainages, generation of microplastics, air pollution, and the release of greenhouse gases [4,5]. To achieve the United Nations Sustainable Development Goals (UN SDGs) by 2030, it is crucial to evaluate policy actions and programs at state, national, and regional levels to address plastic pollution [6].

PET has been used in many applications such as in bottles for beverages and water and packaging materials for foods and textiles [4,7,8]. However, the use of PET poses significant challenges due to its non-biodegradability, thereby leading to the generation of accumulated plastic waste. Consequently, finding sustainable and environmentally friendly methods for proper management of such waste is imperative.

Several conventional methods for plastic waste management have been considered; however, most of these methods have limitations. For instance, recycling plastic waste, which involves melting thermoplastics and remolding it to other products, is not sustainable due to the low-quality products produced [9]. Burning plastics in incinerators is another method of plastic waste management. Nevertheless, this method suffers several limitations, including generating greenhouse gases (CO_2 , CH_4), air pollution, soil contamination, and even posing a threat to human health. Pyrolysis, as a plastic waste management method, offers promising solutions to address the limitations faced by other conventional methods [10,11]. Pyrolysis of plastic waste aligns with SDG 12, which aims to ensure sustainable consumption and production patterns by turning plastic waste into valuable resources. It offers the advantage of converting waste to valuable products such as fuels and other chemical feedstock, minimal environmental impact, job creation, renewable energy production, carbon sequestration, and promoting a circular economy [12,13].

Pyrolysis is a process of breaking down long-chain hydrocarbons into smaller chains with the application of heat and pressure in the absence of oxygen, leading to the formation of valuable products like gases, pyrolysis oils, and char [14]. The liquid oil can be further upgraded to produce fuels (gasoline, C5–C12 and diesel, C13–C20), lubricants, and other valuable chemicals [15]. Typically, pyrolysis involves heating the feedstock to a high temperature range between 400 and 800 °C, resulting in the rupturing of chemical bonds in the feedstock and formation of smaller molecules [16,17]. Pyrolysis is categorized into slow, fast, and flash pyrolysis based on the residence times and heating rates resulting in different product yields and compositions [18,19].

Several studies have been conducted on the pyrolysis of PET, which have shown that it contains saturates and aromatic compounds similar to those found in crude oil. For example, Xue *et al.* [20] carried out pyrolysis of plastics including PET using zeolite catalyst and found that aromatic hydrocarbons were the major products (52.71%) with lower yields of saturates (alkanes and alkenes). In another study, Du *et al.* [21] showed that aromatic hydrocarbons (mostly benzene) were obtained during the pyrolysis of PET carpet waste with ZSM-5 and CaO catalysts to enhance deoxygenation of the products. Suriaparao *et al.* [22] investigated the co-pyrolysis of PET with rice husk and found that it promoted the formation of aromatic oxygenates and biphenyl hydrocarbons. However, the major components obtained in microwave pyrolysis of PET were aromatics. The study also revealed that PET pyrolysis oil contains impurities, tars, a wide distribution of hydrocarbons, and oxygenated compounds, necessitating the need for upgrading such oils using suitable catalysts.

It has been reported that the use of acidic catalysts can aid in cracking and aromatization reactions during the pyrolysis of plastics [23,24]. Additionally, the use of catalysts can decrease the reaction temperature, shorten the reaction time, and reduce the formation of unwanted byproducts [25,26]. Supported iron catalysts have emerged as a promising option for PET pyrolysis, as literature has reported their enhanced efficiency, low cost, and selectivity during the pyrolysis process [27,28].

Although prior works have reported the synthesis of iron–alumina based catalysts [29–32], none have reported the synthesis of iron–alumina based

catalysts from mesoporous FeO derived from natural magnetic sand available locally in Nigeria. Moreover, no work has reported the use of such a catalyst for reforming PET pyrolysis vapor. In this study, a new type of catalyst was developed based on the combination of a novel mesoporous iron oxide synthesized from natural magnetic sand with alumina. The synthesized catalyst was then used to upgrade PET pyrolysis gas into valuable fuels. This study aims to answer the following research questions: first, how does the synthesized catalysts affect the distribution of pyrolysis products of PET after reforming; second, the effect of 3% and 5% FeO catalyst loading on selectivity. The findings of this study will contribute to the development of innovative catalysts and environmentally friendly approaches for PET pyrolysis into valuable fuels.

2. Materials and methods

2.1. Material and equipment

PET was obtained from used drinking water bottles within Zaria, Kaduna State. Prior to the experiment, PET bottle samples were cut into smaller pieces (average size within 2 cm × 2 cm) and allowed to dry in the laboratory. Aluminum oxide trihydrate (alumina) was purchased from Suffolk, England. Iron oxide (prepared from magnetic sand), weighing balance (Kern-EW6000, with an accuracy of 0.001 g), digital hotplate with a magnetic stirrer (Stuart CD162), muffle furnace (SXL-1008 Gallenkamp, England), vacuum pump, hot air oven (Genlab, UK), gas mask, Whatman No. 1 filter paper, distilled water (Water Still Aquatron [A8000] Distiller), and Infrared Syngas Analyzer Gasboard-3100P (Hubei Cubic-Ruiyi Instrument) were utilized. All reagents were used as supplied.

2.2. Catalyst preparation

Mesoporous FeO was incorporated into alumina through the incipient wetness impregnation technique to synthesize 3% and 5% FeO loaded on alumina (3% and 5% FeO/Al). The mesoporous FeO synthesized from magnetic sand according to the method of Gano *et al.* [33] was used to prepare 3% and 5% FeO precursor solution. The predetermined volume of precursor solutions, which is equivalent to



Figure 1. Multifunctional pyrolysis and fixed bed reactor system at NARICT, Zaria.

the pore volume of the alumina, was then carefully added to the support. The mixture was continuously mixed until a homogeneous reddish-brown paste was obtained. The paste was oven-dried at 105 °C overnight, after which it was calcined in a muffle furnace for 3 h at 500 °C.

2.3. Pyrolysis process

PET pyrolysis was conducted using a multifunctional pyrolysis reactor system (PRS) at the National Research Institute for Chemical Technology (NARICT), Zaria (Figure 1). The PRS consisted of a pyrolyzer and fixed bed reactor (FBR; stainless steel tube, 40 cm length, 1 cm internal diameter; Figure 2). Initially, 200 g of PET was charged into the pyrolyzer followed by the passage of nitrogen gas at 0.5 bar for 1 h to create an inert environment. Pyrolysis was then carried out at 350 °C until the pressure in the pyrolyzer reached 10 bar.

While the pyrolyzer pressure was building up, 0.5 g of the catalyst was loaded in between glass wool plug beds inside the FBR. Prior to the start of the catalytic reforming process, N₂ gas was allowed to flow through the reactor at 0.5 bar for 15 min. Subsequently, the catalyst was reduced under H₂ flow at 0.5 bar and 450 °C for 90 min. When the pressure in the pyrolyzer is 10 bar, the bypass valves are opened to allow the pyrolysis vapor to contact the catalyst at 450 °C. At the end of the catalytic reforming process, the product was passed through a condenser into a liquid gas separator tank, where the condensable product is collected while the non-condensable product is directed to an online syngas analyzer

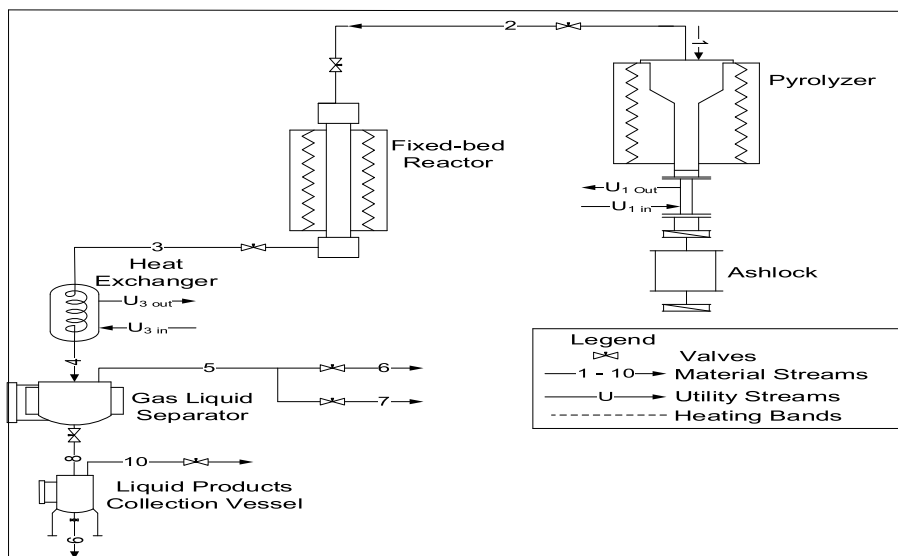


Figure 2. Process flow diagram for the pyrolysis process.

(Hubei Cubic-Ruiyi Instrument) for analysis. The experiment was also conducted using the same condition but without catalyst for comparison.

2.4. Catalyst characterization

Morphology of the samples was performed using a Phenom World scanning electron microscopy (SEM) analyzer (Thermo Fisher, Waltham, US). Infrared data was collected using a Shimadzu-8400S Fourier Transform Infrared Spectrometer (Kyoto, Japan) over the range of $4000\text{--}400\text{ cm}^{-1}$. X-ray diffraction (XRD) measurements were conducted to determine the crystallinity of the sample using a Rigaku MiniFlex X-ray Diffractometer (Texas, USA) with 2θ between 2° and 80° while elemental composition was determined using a Genius IF Xenometrix X-ray fluorescence (XRF) analyzer (Jordan Valley).

2.5. Product characterization

The composition of non-condensable products (gas) was measured using an online syngas analyzer (Hubei Cubic-Ruiyi Instrument). The functional groups in liquid products were determined using an attenuated total reflectance (ATR) mode of Shimadzu-8400S Fourier Transform Infrared Spectrometer (Kyoto, Japan) within the scan range of $600\text{--}4000\text{ cm}^{-1}$. The composition of hydrocarbons

in the liquid sample was determined using Agilent 19091S-433UI GCMS. Data was acquired using a $30\text{ m} \times 250\text{ }\mu\text{m} \times 0.25\text{ }\mu\text{m}$ capillary column flow rate of carrier gas (helium) set to 1.169 mL/min at a flow velocity of 39.404 cm/s . The initial column temperature was set to $50\text{ }^\circ\text{C}$ and held for 5 min, and then ramped to $300\text{ }^\circ\text{C}$ at $10\text{ }^\circ\text{C/min}$ for 20 min. A sample volume of $1\text{ }\mu\text{L}$ was injected using the splitless injection mode at a temperature of $300\text{ }^\circ\text{C}$. The peaks of the resulting chromatographs were identified using the National Institute of Standards and Technology standard reference database.

3. Results and discussion

3.1. Catalyst characterization

3.1.1. SEM analysis

The size and morphology of the catalyst samples were analyzed using SEM analysis, and the results are shown in Figure 3. Alumina particles (Figure 3a) were irregular polyhedrons with angular shapes, which may improve permeability after sintering; see Kim *et al.* [34]. Both 3% FeO/Al and 5% FeO/Al catalysts exhibited a rough, flaky surface with irregularly shaped particles (Figures 3b,c), which were identified as mesoporous FeO deposited on the support after impregnation. The lighter regions in the images are composed primarily of the support while the

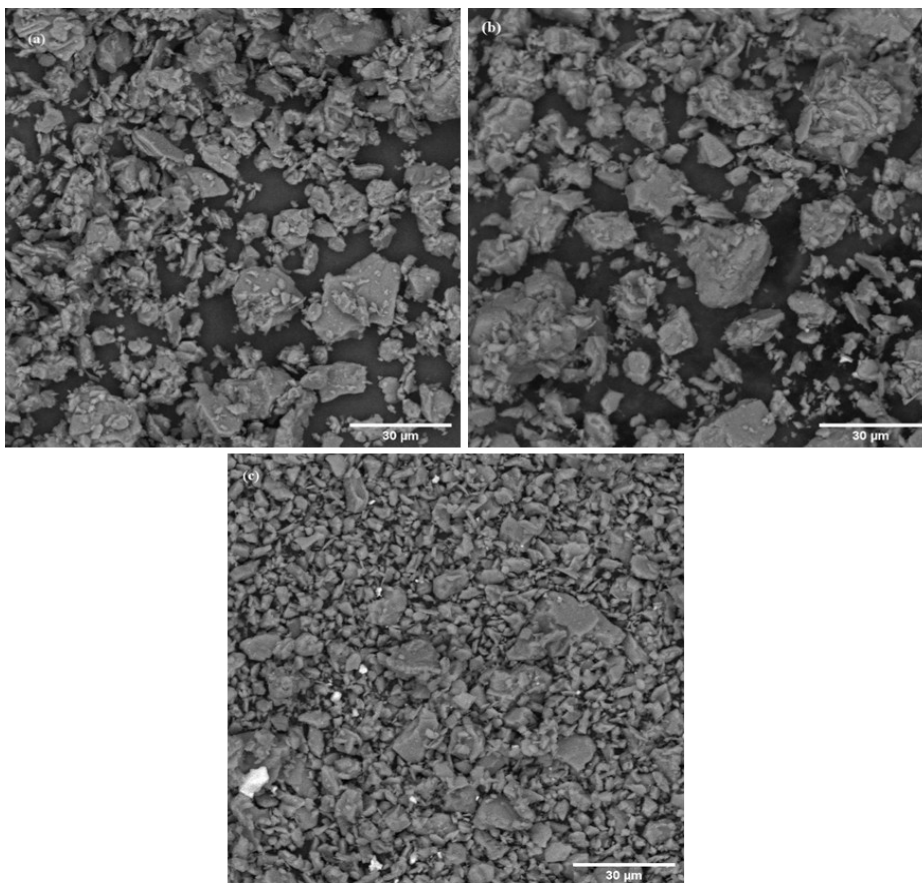


Figure 3. SEM micrograph at $\times 2000$ of (a) alumina, (b) 3% FeO/Al, and (c) 5% FeO/Al.

darker regions are iron particles [29,35]. Additionally, the SEM images revealed many smaller particles dispersed on the surface of the support in 5% FeO/Al, indicating successful dispersion of the mesoporous FeO on the support. These observations confirm the successful synthesis of the catalyst as supported by similar finding in the literature [36].

The particle size analysis (Figure 4) revealed the presence of individual grains detectable at higher magnification ($\times 2000$) to be predominantly in the range of 1.42–7.63, 1.37–10.75, and 2.66–6.34 μm for alumina, 3% FeO/Al, and 5% FeO/Al, respectively. The average particle diameters were 4.45, 4.74, and 3.85 μm for alumina, 3% FeO/Al, and 5% FeO/Al, respectively. The smallest particle size was found in 5% FeO/Al. This suggests that impregnation with mesoporous FeO increased the surface area and therefore, could enhance the catalytic activity due to availability of more active sites for reaction.

3.1.2. XRF analysis

The metal compositions determined by XRF analysis of all the synthesized catalysts and supports are presented in Table 1. As shown in the table, the mesoporous FeO has been successfully incorporated onto the support, with the percentage compositions of Fe detected to be 3.43% and 4.74% for 3% and 5% FeO/Al catalysts, respectively, while Fe detected in alumina was just 0.11%. These compositions are comparable to the metal loadings in the calculation, suggesting that the synthesis process was effective. Moreover, the Al compositions were found to be 45.50%, 47.11%, and 47.90% for 5% FeO/Al, 3% FeO/Al, and alumina (the support), respectively, implying successful impregnation. Other elements were detected in negligible concentrations, signifying fewer impurities in the synthesized catalyst. These findings are consistent with the work

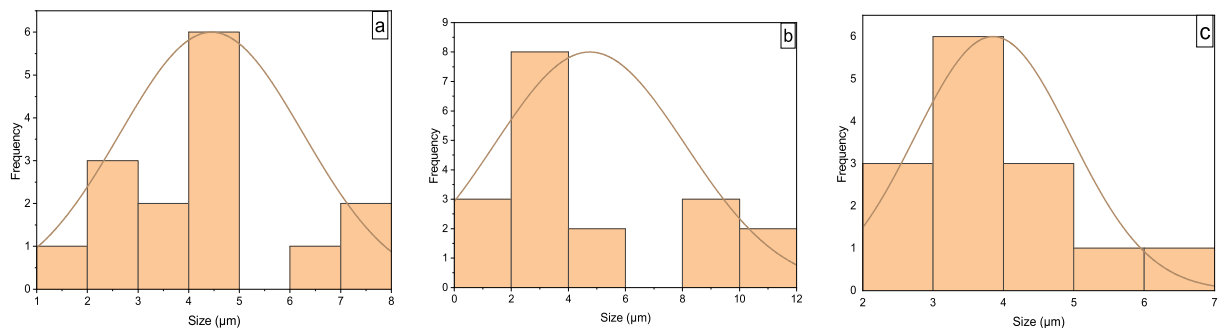


Figure 4. Histogram showing particle size distribution of (a) alumina, (b) 3% FeO/Al, and (c) 5% FeO/Al.

Table 1. Elemental compositions of 3% FeO/Al, 5% FeO/Al, and alumina

Elements	3% FeO/Al (%)	5% FeO/Al (%)	Alumina (%)
Si	1.36	1.52	1.35
Al	47.11	45.50	47.96
Fe	3.43	4.74	0.11
Ti	0.00	0.01	0.03
Ca	0.38	0.16	0.17
P	0.01	0.00	0.01
K	0.00	0.00	0.00
Mn	0.01	0.01	0.01
Mg	0.21	0.75	2.14
Zn	0.04	0.07	0.04

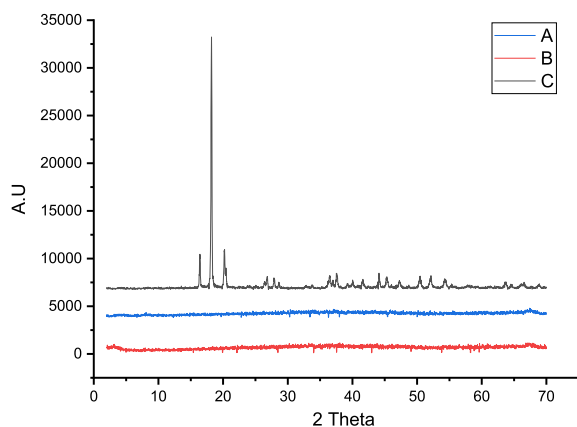


Figure 5. XRD pattern for (a) 3% FeO/Al, (b) 5% FeO/Al, and (c) alumina.

by Tanarungsun *et al.* [37], where Fe and other metals were impregnated onto TiO₂ support.

3.1.3. XRD analysis

The XRD patterns obtained for alumina (a), 3% FeO/Al (b), and 5% FeO/Al (c) are presented in Figure 5. It was observed that the pure alumina was the only crystalline phase identified by the International Centre for Diffraction Data (ICDD). However, the crystallinity of the synthesized catalyst samples was not detected, indicating that the catalyst is amorphous in nature. Amorphous catalysts have been shown to have higher surface areas, more active sites, and enhanced reactivity [38]. Several studies have reported similar results when iron oxide is doped on alumina. For instance, Ramdhani *et al.* [30], Zhong *et al.* [39], and Kamboj *et al.* [40] reported the absence

of crystalline peaks after impregnation of alumina with iron oxide, suggesting the formation of an amorphous phase. The formation of a non-crystalline phase when FeO is impregnated on alumina could be because of high dispersion of Fe on the surface of the catalyst as reported in a previous study [30]. Another factor that could affect the crystallinity of the synthesized catalyst is the calcination temperature (450 °C). Several researchers have reported higher crystallinity for iron oxide doped on alumina at higher temperatures in the range of 500–1000 °C [39,41].

3.2. Product analysis

3.2.1. Analysis of gaseous products

Gaseous products were analyzed using an on-line gas analyzer after exposure to different catalysts.

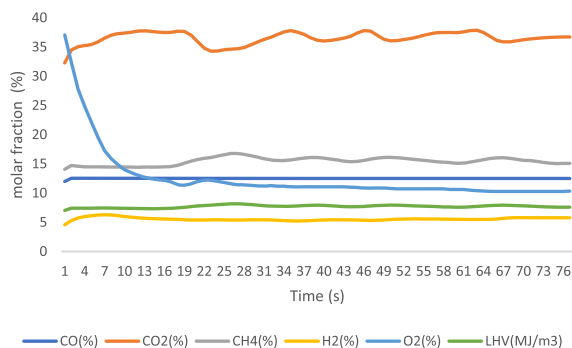


Figure 6. Gas analysis of reformed PET pyrolysis vapor using 3% Fe/Al catalyst.

The obtained results are presented in Figures 6–8 for 3% FeO/Al, 5% FeO/Al, and blank run, respectively. The compositions of the components were reported when the readings from the analyzer stabilized, with values expressed as molar fractions in percentage (%). Oxygen content decreased from 23.3% in the blank run to 10.96% and 5.33% in 3% FeO/Al and 5% FeO/Al, respectively, indicating a decrease in oxygenated compounds when the synthesized catalyst was used. The H₂ content was highest in 5% FeO/Al, with a value of 17.14%. Conversely, the CH₄ content was highest in 3% FeO/Al (16.22%) and lowest in 5% FeO/Al (12.11%). The CO value decreased from 14.02% in the blank run to 12.51% and 12.64% in 3% FeO/Al and 5% FeO/Al, respectively, indicating an improvement in the synthesized catalyst. The CO₂ value was found to be 20.96%, 30.03%, and 36.86% for the blank run, 5% FeO/Al, and 3% FeO/Al, respectively. Furthermore, the low heating value was found to be 6.41, 7.72, and 7.84 MJ/m³ for the blank run, 3% FeO/Al, and 5% FeO/Al, respectively. Similar findings was reported by Dhahak *et al.* [42] and Li *et al.* [43]. It is evident that the presence of the catalyst has improved the overall quality of the gas by reducing the O₂ content, and increasing the syngas (H₂/CO) and methane contents. These results demonstrated the effectiveness of the synthesized catalyst in reforming the pyrolysis gas.

3.2.2. Analysis of liquid products

Fourier transform infrared-ATR (FTIR-ATR) spectroscopy and gas chromatography mass spectrometry (GCMS) techniques were used to study the functional groups and hydrocarbon composition of the

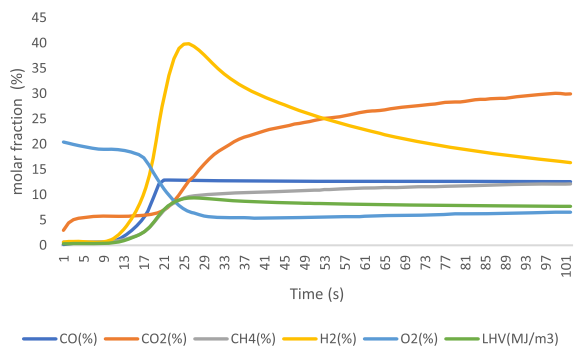


Figure 7. Gas analysis of reformed PET pyrolysis vapor using 5% Fe/Al catalyst.

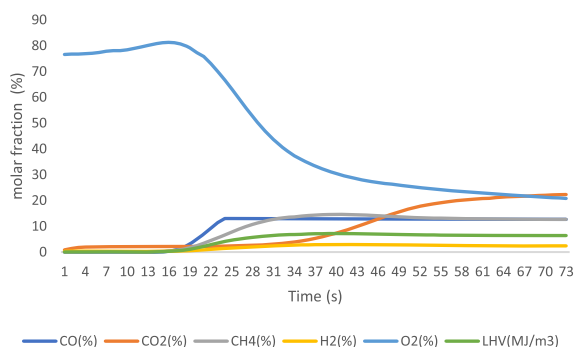


Figure 8. Gas analysis of pyrolysis vapor in blank run.

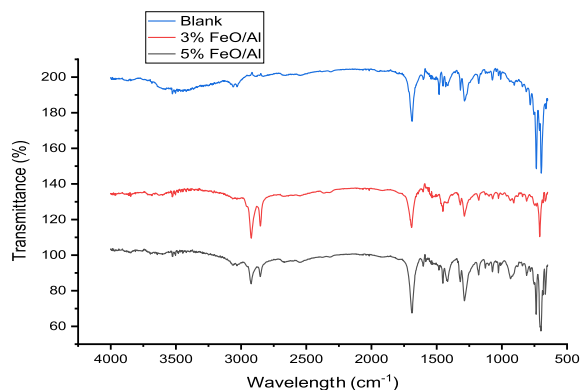
liquid products obtained before and after reforming using 3% and 5% FeO/Al catalysts. The FTIR spectra of the liquid product are shown in Figure 9 while the major functional groups are presented in Table 2 with their corresponding assignments. The results showed that the catalysts were able to reform PET vapor into aliphatic alkanes as can be seen by the presence of peaks at 2988 and 2899 cm⁻¹, which were absent in the blank run. Additionally, the peaks at 929, 1290, 1420, and 1689 cm⁻¹ appeared to be more prominent in the reformed product using 5% FeO/Al catalyst, suggesting an increase in the quantity of aromatics. This underscores the excellent performance of the synthesized catalyst. A similar result has been reported in a previous study by Nasution *et al.* [44].

The analysis of liquid products by GCMS provided insight into the composition of hydrocarbons present with and without the catalyst. The composition of hydrocarbons present in the samples is summarized

Table 2. FTIR assignments for liquid products obtained for blank run and after catalytic reforming of pyrolysis vapor

Peaks (cm ⁻¹)	Blank run	3% FeO/Al	5% FeO/Al	Type of vibration	Nature of functional group
3050	✓	✓	✓	C–H stretching	Unsaturated aromatic
2924	×	✓	✓	C–H stretching	Aliphatic alkanes
2854	×	✓	✓	O–H stretching	Alcohols
1689	✓	✓	✓	C=O stretching	Alkenes
1420	✓	✓	✓	C–H stretching	Aromatic ring
1292	✓	✓	✓	C–H scissoring and bending	Alkene
1180	✓	✓	✓	C–O stretching	Alcohols, esters, carboxylic acids
923	✓	✓	✓	C–H bending	Alkene
713	✓	×	✓	C–H bending	Alkene, phenyl ring substitution
713	✓	✓	✓	C–H bending	Alkene, phenyl ring substitution

Key: ✓ = present, × = absent.

**Figure 9.** FTIR spectra of liquid product for blank run and after catalytic reforming of pyrolysis vapor.

in Table 3 while the GCMS chromatogram is presented in Figure 10. The results showed a significant change in hydrocarbon composition between the blank run and the reformed products. All the samples contained mixtures of aliphatic and aromatic hydrocarbons. However, increasing the percentage of mesoporous FeO impregnated in the catalyst (from 3% to 5% FeO) facilitated a selective catalytic reforming process as seen in the significant reduction of peaks from the blank run to that in the 5% FeO/Al sample. This led to a reduction in the formation of undesirable byproducts such as ketones, alcohols, esters, and acidic compounds, which were found in significant amounts in the blank run. These

findings are in agreement with the work of Aisein *et al.* [45], Nasution *et al.* [44], and Rotta *et al.* [46]. Moreover, the data obtained substantiates the presence of aromatics and aliphatic hydrocarbons as inferred by the FTIR results. The findings indicated that the synthesized catalyst could transform complex pyrolysis vapor containing a wide range of products into a more streamlined composition of hydrocarbons. Similar results have been reported by Malik *et al.* [47].

4. Conclusion

This study investigated the pyrolysis of PET into fuel using synthesized mesoporous FeO-based catalysts (3% FeO/Al and 5% FeO/Al). Analyses using SEM, XRF, and XRD revealed the catalyst's well-defined morphological, structural, and compositional properties. Reforming using catalysts reduced oxygen content whereas CH₄ and H₂ contents were improved in the gaseous products. FTIR and GCMS analyses of liquid products demonstrated the catalyst's ability to reform pyrolysis vapor into valuable products.

These findings highlight the potential of mesoporous FeO-based catalysts in converting PET waste into valuable fuel products. This research contributes to the management of plastic waste by providing an alternative pathway for its conversion into useful products.

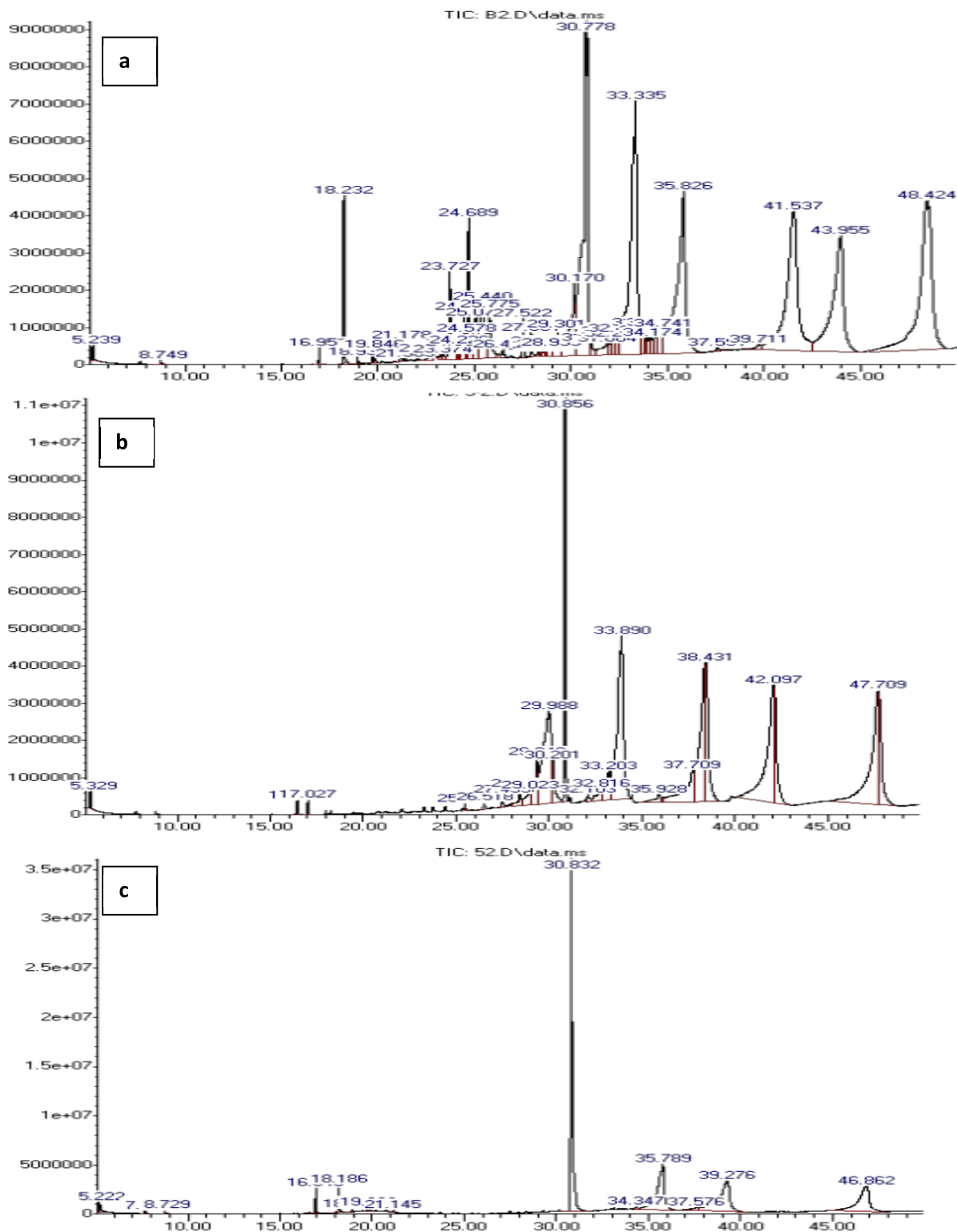


Figure 10. GCMS analysis of liquid products from catalytic reforming process (a) blank run, (b) 3% FeO/Al and (c) 5% FeO/Al.

Table 3. Composition of liquid product obtained for blank run and after catalytic reforming of pyrolysis vapor

Blank run	Relative area	3% FeO/Al	Relative area	5% FeO/Al	Relative area
Cyclohexane, methylene-	0.1244	Cycloeicosane	1.1838	Norbornane	0.5448
1,1'-Bicyclohexyl	0.1193	1-Chloroeicosane	2.1595	Benzene, chloro-	0.1316
Biphenyl	1.2557	Octadecane, 1-(ethenyloxy)-	11.0148	Cyclohexanol	0.1455
1,1'-Biphenyl, 3-methyl-	0.1059	Eicosane, 9-cyclohexyl-	1.2875	1,1'-Bicyclohexyl	1.2929
1,1'-Biphenyl, 4-methyl-	0.1236	Bis(2-ethylhexyl) phthalate	8.3623	Biphenyl	1.6627
Fluorene	0.2151	Octacosanal	0.9057	Fluorene, 2,4a-dihydro-	0.153
(E)-Stilbene	0.1875	Methoxyacetic acid, heptadecyl ester	1.7296	1,1'-Biphenyl, 4-methyl-	0.2786
9-Hexadecenoic acid	0.1144	9,12- Octadecadienoyl chloride, (Z,Z)-	15.3116	Fluorene	0.1634
Phenanthrene, tetradecahydro-	0.1218	Methoxyacetic acid, heptadecyl ester	4.1935	Diisooctyl phthalate	33.7527
Phenanthrene	1.4882	6-Nitroundec-5-ene	10.4797	Carbonic acid, octadecyl prop-1-en-2-yl ester	0.2488
2-Methyl-Z,Z-3,13- octadecadienol	0.1339	10-Methyl-E-11- tridece-1-ol acetate	6.2048	Octacosane	21.1329
9,12- Octadecadienoic acid (Z,Z)-	0.2398	9-Octadecynenitrile	12.0354	Erucic acid	1.0636
Naphthalene, 1-phenyl-	0.8766	7,11-Hexadecadienal	4.9289	9,12- Octadecadienoyl chloride, (Z,Z)-	21.1182
Anthracene, 1-methyl- o-Terphenyl	0.2604 1.9577	9-Octadecenal 9,12- Octadecadienoyl chloride, (Z,Z)-	11.8024 5.6292	9-Octadecenal -	18.0856 -
Phenanthrene, 4-methyl-	1.4162	-	-	-	-
Heptadecane	2.1588	-	-	-	-
Naphthalene, 2-phenyl-	1.1002	-	-	-	-
Heneicosane	0.1318	-	-	-	-
m-Terphenyl	0.4636	-	-	-	-
p-Terphenyl	0.2767	-	-	-	-
1-Chloroeicosane	0.1083	-	-	-	-

(continued on next page)

Table 3. (continued)

Blank run	Relative area	3% FeO/Al	Relative area	5% FeO/Al	Relative area
2-Propenoic acid, 2-cyano-3-(4-dimethylaminophenyl)-, ethyl ester	0.1069	–	–	–	–
Spiro[2.3]hexan-4-one, 5,5-diethyl-	0.1214	–	–	–	–
9,12-Octadecadienal	0.2133	–	–	–	–
1-Chloroeicosane	0.8156	–	–	–	–
Eicosane	3.0545	–	–	–	–
Diisooctyl phthalate	13.8353	–	–	–	–
Eicosane	0.2271	–	–	–	–
9-Methyl-10,12-hexadecadien-1-ol acetate	0.7105	–	–	–	–
Carbonic acid, eicosyl vinyl ester	0.31	–	–	–	–
Hexadecane, 1-(ethenyl)-	0.331	–	–	–	–
Hexadecane, 1-(ethenyl)-	0.5	–	–	–	–
Phthalic acid, isohexyl neopentyl ester	13.803	–	–	–	–
Bis-(3,5,5-trimethylhexyl) phthalate	0.4155	–	–	–	–
1,2-Benzenedicarboxylic acid, monobutyl ester	0.3703	–	–	–	–
Erucic acid	0.3204	–	–	–	–
Eicosane	0.5716	–	–	–	–
6-Nitroundec-5-ene	0.8206	–	–	–	–
Cycloeicosane	10.9885	–	–	–	–
Cycloeicosane	0.2487	–	–	–	–
9-Octadecenal	13.0695	–	–	–	–
9,12-Octadecadienal	10.4876	–	–	–	–
(Z)-1,3-Dimethoxypropan-2-yl docos-13-enoate	15.4166	–	–	–	–

Declaration of interests

The authors do not work for, advise, own shares in, or receive funds from any organization that could benefit from this article, and have declared no affiliations other than their research organizations.

Funding

The authors appreciate the NARICT for the financial and technical support rendered in carrying out

this research under project number FGN/AB2021/ERGP30122610.

References

- [1] U. N. P. Fund, *World Population Dashboard*, Saudi Arabia, 2022.
- [2] T. Sogbanmu, *The Conversation*, 2022, Available from: <https://theconversation.com/plastic-pollution-in-nigeria-is-poorly-studied-but-enough-is-known-to-urge-action-184591>.

- [3] T. Obiezu, *Nigerian Recyclers Reduce Plastic Waste By Exchanging Trash for Cash*, Voice of America, 2019, Retrieved March. Available from: <https://www.voanews.com/africa/nigerian-recyclers-reduce-plastic-waste-exchanging-trash-cash#:~:text=Nigerian%20Recyclers%20Reduce%20Plastic%20Waste%20by%20Exchanging%20Trash%20for%20Cash,-By%20Timothy%20Obiezu&text=ABUJA%2C%20NIGERIA%20%2D%20Nigeria%20ge>.
- [4] O. A. Alabi, K. I. Ologbonjaye, O. Awosolu, O. E. Alalade, *J. Toxicol. Risk Assess.*, 2019, **5**, 1-13.
- [5] R. Verma, K. Vinoda, M. Papireddy, A. Gowda, *Proc. Environ. Sci.*, 2016, **35**, 701-708.
- [6] B. Yalwaji, H. O. John-Nwagwu, T. O. Sogbanmu, *Sci. Afr.*, 2022, **16**, article no. e01220.
- [7] Y. Liu, W. Fu, T. Liu, Y. Zhang, B. Li, *J. Anal. Appl. Pyrol.*, 2022, **161**, article no. 105414.
- [8] A. Brems, J. Baeyens, C. Vandecasteele, R. Dewil, *J. Air Waste Manag. Assoc.*, 2011, **61**, 721-731.
- [9] J. Aguado, D. Serrano, G. San Miguel, J. Escola, J. Rodríguez, *J. Anal. Appl. Pyrol.*, 2007, **78**, 153-161.
- [10] S. Al-Salem, A. Antelava, A. Constantinou, G. Manos, A. Dutta, *J. Environ. Manag.*, 2017, **197**, 177-198.
- [11] N. Sakthipriya, *Sci. Total Environ.*, 2022, **809**, article no. 151160.
- [12] A. T. Hoang, P. S. Varbanov, S. Nižetić, R. Sirohi, A. Pandey, R. Luque, K. H. Ng, *J. Cleaner Prod.*, 2022, **359**, article no. 131897.
- [13] S. Kartik, H. K. Balsora, M. Sharma, A. Saptoru, R. K. Jain, J. B. Joshi, A. Sharma, *Therm. Sci. Eng. Prog.*, 2022, **32**, article no. 101316.
- [14] K. Sivagami, K. V. Kumar, P. Tamizhdurai, D. Govindarajan, M. Kumar, I. Nambi, *RSC Adv.*, 2022, **12**, 7612-7620.
- [15] M. H. Rahman, P. R. Bhoi, P. L. Menezes, *Renew. Sustain. Energy Rev.*, 2023, **188**, article no. 113799.
- [16] A. Al-Rumaihi, M. Shahbaz, G. Mckay, H. Mackey, T. Al-Ansari, *Renew. Sustain. Energy Rev.*, 2022, **167**, article no. 112715.
- [17] A. T. Hoang, H. C. Ong, I. R. Fattah, C. T. Chong, C. K. Cheng, R. Sakthivel, Y. S. Ok, *Fuel Process. Technol.*, 2021, **223**, article no. 106997.
- [18] B. Adelawon, G. Latinwo, B. Eboibi, O. Agbede, S. Agarry, *Chem. Eng. Commun.*, 2022, **209**, 1246-1276.
- [19] R. K. Mishra, K. Mohanty, *Liquid Biofuels: Fundamentals, Characterization, and Applications*, John Wiley & Sons, 2021, 231-284 pages.
- [20] Y. Xue, P. Johnston, X. Bai, *Energy Convers. Manag.*, 2017, **142**, 441-451.
- [21] S. Du, J. A. Valla, R. S. Parnas, G. M. Bollas, *ACS Sustain. Chem. Eng.*, 2016, **4**, 2852-2860.
- [22] D. V. Suriapparao, D. A. Kumar, R. Vinu, *Sustain. Energy Technol. Assess.*, 2022, **49**, article no. 101781.
- [23] W. Luo, Q. Hu, Z.-y. Fan *et al.*, *Energy*, 2020, **213**, article no. 119080.
- [24] D. Serrano, J. Aguado, J. Escola, *Acs Catal.*, 2012, **2**, 1924-1941.
- [25] T.-T. Meng, H. Zhang, F. Lü, L.-M. Shao, P.-J. He, *J. Anal. Appl. Pyrol.*, 2021, **159**, article no. 105312.
- [26] J. Sun, J. Luo, J. Lin, R. Ma, S. Sun, L. Fang, H. Li, *Energy*, 2022, **247**, article no. 123547.
- [27] N. Cai, S. Xia, X. Li *et al.*, *Waste Manag.*, 2021, **136**, 47-56.
- [28] B. Ramadhani, T. Kivevele, J. H. Kihedu, Y. A. Jande, *Biomass Convers. Biorefin.*, 2020, **12**, 1369-1392.
- [29] S. Mosallanejad, B. Z. Dlugogorski, E. M. Kennedy, M. Stockenhuber, *ACS Omega*, 2018, **3**, 5362-5374.
- [30] E. P. Ramdhani, E. Santoso, H. Holilah *et al.*, *RSC Adv.*, 2023, **13**, 31989-31999.
- [31] X. Shen, Z. Zhao, H. Li, X. Gao, X. Fan, *Mater. Today Chem.*, 2022, **26**, article no. 101166.
- [32] N. Cai, X. Li, S. Xia *et al.*, *Energy Convers. Manag.*, 2021, **229**, article no. 113794.
- [33] Z. S. Gano, E. A. Audu, A. A. Osigbesan, A. F. Ade-Ajayi, J. T. Barminas, *Inorg. Chem. Commun.*, 2024, **159**, article no. 111854.
- [34] J. Kim, J.-H. Ha, J. Lee *et al.*, *J. Korean Ceram. Soc.*, 2017, **54**, 331-339.
- [35] M. M. Mohamed, W. Bayoumy, H. El-Faramawy, W. El-Dogdog, A. A. Mohamed, *Renew. Energy*, 2020, **160**, 450-464.
- [36] F. Gulshan, K. Okada, *J. Eng. Res.*, 2015, **3**, article no. 10.
- [37] G. Tanarungsun, W. Kiatkittipong, P. Praserttham, H. Yamada, T. Tagawa, S. Assabumrungrat, *J. Ind. Eng. Chem.*, 2008, **14**, 596-601.
- [38] G. Chen, Y. Zhu, H. M. Chen *et al.*, *Adv. Mater.*, 2019, **31**, article no. 1900883.
- [39] Z. Zhong, T. Prozorov, I. Felner, A. Gedanken, *J. Phys. Chem. B*, 1999, **103**, 947-956.
- [40] N. Kamboj, A. S. Shamsheer, E. V. Shirshneva-Vaschenko, I. Hussainova, *Mater. Chem. Phys.*, 2019, **225**, 340-346.
- [41] A. O. Ali, A. M. El Naggat, A. S. Morshedy, W. A. Aboutaleb, N. H. Metwally, *Chemosphere*, 2022, **307**, article no. 136011.
- [42] A. Dhahak, G. Hild, M. Rouaud, G. Mauviel, V. Burkle-Vitzthum, *J. Anal. Appl. Pyrol.*, 2019, **142**, article no. 104664.
- [43] Y. Li, M. A. Nahil, P. T. Williams, *Chem. Eng. J.*, 2023, **467**, article no. 143427.
- [44] F. Nasution, H. Husin, F. Abnisa, F. T. Yani, L. Maulinda, *Energy Convers. Manag.*, 2022, **273**, article no. 116440.
- [45] F. A. Aisien, E. T. Aisien, *Sustain. Chem. Clim. Action*, 2023, **2**, article no. 100020.
- [46] A. N. Rotta, C. Bota, B. Brem, D. I. Porumb, E. Gal, *Stud. Univ. Babeş-Bolyai, Chem.*, 2022, **67**, 169-185.
- [47] S. Malik, H. Gulab, K. Hussain, M. Hussain, M. Haleem, *Int. J. Environ. Sci. Technol.*, 2022, **19**, 4019-4036.